Evolution of chemical species during electrodeposition of uranium for alpha spectrometry by the Hallstadius method

A.M. Beesley, M.T. Crespo, N. Weiher, N. Tsapatsaris, J.S. Cózar, H. Esparza, C.G. Méndez, P. Hill, S.L.M. Schroeder, M.E. Montero-Cabrero

Abstract

The morphology and composition of uranium alpha sources with co-deposited platinum have been investigated by scanning electron microscopy (SEM) with energy dispersive X-ray fluorescence analysis (EDX), X-ray photoelectron spectroscopy (XPS) and X-ray absorption fine structure (XAFS) studies. Combined SEM and EDX measurements reveal the effect of porous platinum on the morphology of the sources which in turn affects their alpha-spectral resolution. The XPS analysis suggests that the presence of platinum initially increases the concentration of hydroxyl species in the deposits, which then act as centres for subsequent preferential uranium precipitation. XPS and XAFS analysis also provide for first time an indication of oxidation states of uranium present in the sources prepared by the Hallstadius method. These results are in line with Hansen's theory of electrodeposition of actinides.

Keywords: Uranium, Source preparation, Alpha-spectrometry, Electrodeposition, SEM-EDX, XPS, XANES, EXAFS, Oxidation states.

Introduction

Alpha spectrometry is a radiometric technique that has found many applications in diverse fields such as environmental and geological studies (Crespo et al., 2003; Danesi et al., 2003; Renteria Villalobos et al., 2007), characterization of nuclear wastes (Sill, 1987; Gascon et al., 1994; Rubio Montero et al., 2004; Arimoto et al., 2005)

nuclear decay data measurements (Garcia-Torano et al., 2005) and those related to health and security (Alonso-Hernandez et al., 2002; Yamamoto et al., 2002; Álvarez et al., 2005; Minteer et al., 2007).

Suitable sources for alpha spectrometry must be thin and uniform in order to obtain high energy resolution spectra and to produce accurate measurements. Electrodeposition is the most common technique of source preparation for routine measure-ments (Vera Tomé and Martin Sánchez, 1991; Tsoupko-Sitnikov et al., 2000; Garcia-Torano, 2006). Alpha sources prepared by this method consist of a radioactive deposit onto a metallic substrate (cathode of the electrolytic cell), commonly stainless steel. According to Hansen (1959), the electrodeposition from aqueous media of uranium and other actinides occurs by a precipitation reaction within a hydroxyl ions layer formed at the cathode surface. Considerable effort has been made to study the theoretical and experimental conditions for this process to optimize the electrodeposition setup and the parameters affecting the yield and energy resolution of the sources (Vera Tomé and Martin Sánchez, 1991; Vera Tome´ et al., 1994; Becerril-Vilchis et al., 1996; Lee and Lee, 2000; Tsoupko-Sitnikov et al., 2000).

From the literature, radioactive deposits made by the well known and extensively used Hallstadius method (1984) were examined by Rutherford backscattering and X-ray fluorescence analysis (Ferrero Calabuig et al., 1996, 1998a), which demonstrated the inhomogeneity of ^{232} and natural uranium sources prepared by the Hallstadius method and revealed the presence of co-deposited platinum, which originates from the dissolution of the anode during the electrodeposition process (Ota et al., 1988). Using scanning electron microscopy (SEM) and energy-dispersive X-ray fluorescence (EDX),

Weber et al. (1999) examined uranium electrodeposited sources (30 μg/cm^2) prepared by this method and found that the deposits consisted of spheres containing uranium and platinum, with a diameter depending on the quality of the polishing of the substrate. It was also suggested that dissolved platinum may act as a carrier for the actinide elements during deposition. In this sense, Ferrero Calabuig et al. (1998b) found that uranium was electro deposited even when semipermeable membranes were used to prevent the Pt atoms reaching the cathode, although electrodeposition yields with the membranes were significantly lower. Surface in homogeneity of the sources was further confirmed by Martín Sánchez etal.(2002a,b) by means of scanning probe microscopy and atomic force microscopy.

In the present work, the Hallstadius method (1984),a modification of Talvitie's method (1972), for the electrodeposition of actinides has been used to prepare natural uranium sources. We report the results of a study designed to obtain more information on the morphology and spatial distribution of the U/Pt deposits on stainless steel substrates with the associated chemical speciation of uranium. The surface morphology and composition of the electrodeposits were obtained by SEM coupled to an EDX analytical system. The activity of the samples has been measured by alpha spectrometry and the oxidation state of the species at the surface has been investigated by X-ray photoelectron spectro-scopy (XPS) and X-ray absorption fine structure spectroscopy (XAFS). XAFS has also been carried out to provide an insight into the coordination structure of uranium species in the deposits. Based on our results we attempt to shed light onto the evolution of chemical species during the Hallstadius electrodeposition process, within the Hansen approach.

Experimental

All samples were prepared by the Hallstadius (1984) method at CIEMAT from a CIEMAT natural uranium standard solution of 6.15±0.15 Bq/g activity concentration. The Hallstadius method uses a sulphuric acid electrolyte with Na_2SO_4 to prevent the adsorption of the low mass concentration of most actinides onto the wall of the electrodeposition cell. The pH of the electrolyte is adjusted to 2.1–2.4. In our experimental setup, the deposition was performed onto mirror polished stainless steel (SS) disks (2.5 cm diameter, 1 mm thickness), which acted as the cathodes of the electrolysis cell, while the anode was a platinum wire. During deposition a current density of 0.52 A cm^{-2} and 7mm distance between electrodes was used. This resulted in a deposit covering an area of approximately 2.2 cm diameter.

The Pt anode was a 1 mm diameter wire folded in the base into spiral shape. Only the lower part of the straight wire and the spiral were submersed in the electrolyte. The diameters of the straight non-submersed and submersed parts of the anode wire were measured at various points and the mean values and standard deviations were found to be 0.9875±0.0031 and 0.9686± 0.0024 mm, respectively. This electrode has been used for years in the preparation of uranium sources. These values ensure the slow dissolution of the platinum anode in contact with the electrolyte, confirmed by optical microscopy.

Three sets of sources were prepared, each with electrodeposi-tion times between 20 and 60 min. One set was performed in the absence of uranium in the electrolyte (blank samples) and the other two with the addition of uranium. Table 1 summarizes the resulting sources, including their uranium content.

Alpha spectrometry is commonly used to obtain the isotopic composition of this element in different matrixes and the low specific activity of the main isotope of this element, ^{238}U, allows obtaining significant mass in the deposit, suitable to our studies. Alpha spectrometry has been performed at Manchester with a 100 mm^2 PIPS detector (12 keV nominal resolution quoted by the manufacturer) lodged in a CANBERRA 7401 alpha spectrometer and a source-to-detector distance of 25 mm. For each experiment, a complete spectrum of 4096 channels was accumulated, each channel corresponding to an energy interval of 2.2 keV. In order to obtained information regarding resolution of the sources, the counting time was set to 36 h.

Table 1
Characteristics of sources studied in this work.

Sample	Time of electrodeposition (min)	Main composition	Uranium mass (μg)
Blank 20	20	Pt	
Blank 40	40	Pt	
Blank 60	60	Pt	
U1520	20	U+Pt	128
U540	40	U+Pt	131
U1460	60	U+Pt	153
U1220	20	U+Pt	130
U430	30	U+Pt	120
U1340	40	U+Pt	134
U1760	60	U+Pt	148

The morphology of the samples was studied and confirmed at three different laboratories: at Manchester, using an environ-mental scanning electron microscope (ESEM) FEI Quanta 200, coupled to an EDX system; at CIEMAT, using a Zeiss DSM

960 instrument coupled to its EDX system Link eXL; and at CIMAV, using a scanning electron microscope JEOL JSM-5800 LV coupled to an EDX.

In order to characterize the chemical composition of the electrodeposited sources, XPS and XAFS analysis were performed. XPS probes elemental composition of the surface and gives information about oxidation state of elements (O'Connor et al., 2003). Studies on the uranium coordination species in the deposits were carried out by XAFS. XAFS spectroscopy is a well-established technique that probes local molecular structure providing information about the geometry and electronic struc-ture around the absorbing atom (Koningsberger and Prins, 1988).

Surface elemental analysis by means of XPS was carried out using a Kratos Axis Ultra spectrometer at Manchester. The instrument comprises a monochromated Al K_{α} source, a hybrid electrostatic and magnetic lens system, and charge neutralisation. Pass energies of 80 and 20 eV were used for acquiring survey and high resolution spectra, respectively. All scans were measured with grounded samples, for survey data from kinetic energy of 1100 to 5 eV beyond the cut-off at the Fermi level of the spectrometer, and with 0.5 eV steps between and 200 ms dwell time per data point. The high resolution scans were taken around the emission lines of interest using 0.1 eV steps and 300 ms dwell times per data point, with two repeats. The analytical area of detection was a circular spot with approximately 1 mm diameter. The analysis of the data was carried out using the commercial CasaXPS package (Fairley, 1999–2002). The energetic position of the maximum in the C1s emission line from spurious carbon contamination (binding energy: 284.8 eV) was used to calibrate the energy scale of the spectra.

XAFS experiments at the UL_3-edge were carried out at the STFC Daresbury Synchrotron Radiation Source (SRS) at station 9.3. The SRS storage ring was operated at 2.0 GeV with a beam current of 150–220 mA. We used a Si(2 2 0) double crystal monochromator. The beam size was 1.0 mm x 3.0 mm. XAFS U L_3 spectra were acquired in total electron yield mode using the collector and sample currents, and in fluorescence-yield mode using a 9-element Ge solid state detector. Data were recorded on an energy grid of 10 eV/step in the pre-edge region and 0.5 eV/step in the remaining X-ray absorption near edge spectra (XANES) region, with an integration time of 1 s/step. The extended X-ray absorp-tion fine structure (EXAFS) region was scanned in k-scan mode from 3.1 to 12 $Å^{-1}$ using k-steps of 0.05 $Å^{-1}$ and an integration time increasing from 1 s per step to 10 s per step at the end of the k-scan. Total acquisition time was ~40 min per spectrum. An energy calibration of the beam was performed by collecting the transmission spectra of a reference Zr foil at the Zr K edge. A set of 9 to 10 spectra were taken for each sample and averaged for increasing signal-to-noise ratio.

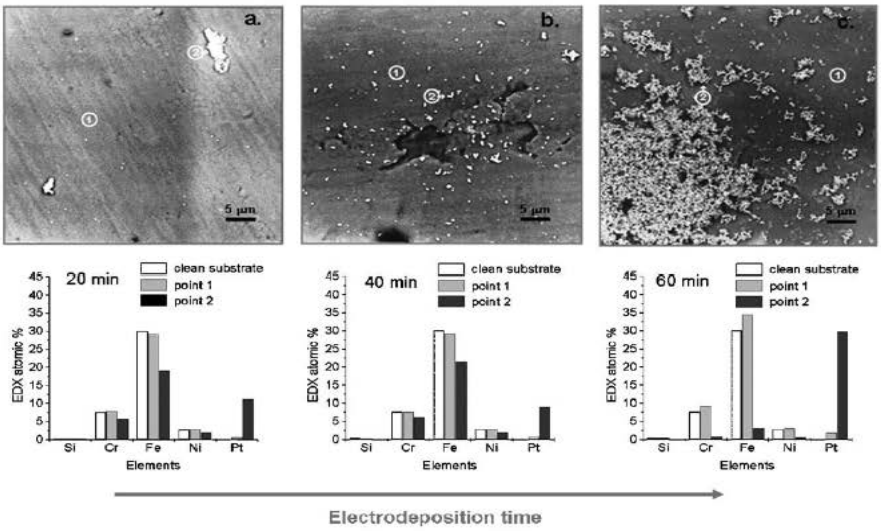

Fig. 1. SEM images and quantification results of the EDX analysis of Pt distribution in blank samples obtained at different electrodeposition times of (a) 20 min, (b) 40 min and (c) 60 min with no radioactive electrolyte.

Results and discussion

SEM-EDX: Three sources, Blank-20, Blank-40 and Blank-60, were prepared at different electrodeposition times of 20, 40 and 60 min from an electrolyte free of radioactive material. Fig. 1 shows SEM images and EDX semiquantitative results of a clean SS substrate and the blank samples. It can be observed that there is a progressive increase of solid aggregates on the surface of the substrate, in particular when the electrodeposition time rises from 40 to 60 min. EDX analysis on the smooth surface parts of the image (points 1) show only the contribution from the SS components of the substrates. EDX analysis on the solid aggregates (points 2) show the SS components along with platinum dissolved from the anode growing on the substrate surface. Dissolution of platinum anodes in sulphuric acid electrolytes has been reported by Ota et al. (1988). The morphology of the platinum precipitate is similar to that obtained using different electrochemical deposition methods such as molten-salt electrolysis (Serrano et al., 2000). Electrolytic metal deposits can develop several morphologies such as dendrites, flakes, needles, fibrous or spongy forms, depending on the electrodeposition parameters and on the nature of the metal (Pavlovic and Popov, 2005). The appearance of the platinum deposits of Fig. 1 is commonly described as moss-like or mossy morphology, typically observed in other electrodeposited metals such as zinc (Wang et al., 2006).

Seven U sources (see Table 1) were prepared at different electrodeposition times of 20, 30, 40 and 60 min. Fig. 2 shows low magnification SEM images of some of these deposits and their comparison with the corresponding blanks, as well as the EDX semiquantitative average taken from different regions in equivalent sources. It can be

observed that uranium deposition initially occurs in the form of clusters, following a similar trend to that of platinum in the blanks. This fact suggests a probable increase of the hydroxyl concentration in the porous deposited platinum with the subsequent preferential precipitation of the uranium at these points (Hansen, 1959). These clusters are progressively covered to form a more homogeneous uranium deposit. Fig. 3 shows detailed images of the sources. Averages of EDX analysis at different points on the sources shown in Figs. 2 and 3 confirm the joint presence of platinum and uranium with ratios Pt/U>1. Magnification of one cluster from sample U17-60 is shown in Fig. 4. This figure reveals newly formed spherulitic structures, similar to those described by Weber et al. (1999) and those obtained in the preparation of U from chloride melts (Serrano et al., 2000), which evolve to colloidal-like crusts with shrinkage cracks, structure that is also commonly observed in the precipitation of low temperature U(IV)+U(VI) oxyhydroxides (UO_{2+x})(Ramdohr, 1969; Perez del Villar et al., 2002). Confirmation of the chemical composition of the deposits requires techniques with higher surface sensitivity than EDX.

Speciation of uranium and platinum in the deposits as function of time:

X-ray photoelectron spectroscopy: In contrast to EDX, XPS has much higher surface sensitivity (probing depth in the nm rather than mm range) (O'Connor et al., 2003). The analysis of all observed peak intensities in the survey XP spectra allows a quantification of the elemental composition of the surface region probed by XPS. We analysed the surfaces of four samples: U12-20, U4-30, U13-40 and U17-60, corresponding to 20, 30, 40 and 60 min electrodeposition time (see Table 1). The results of this analysis are summarised in Table 2. SEM-EDX trend results show that

the amount of platinum increases with electrodeposition time, hence the most striking feature of Table 2 is the small amount of platinum found in the surface of source U13-40. This is also in accordance with that found in the alpha spectrometric measurement of this source (see below). This suggests that a little fortuitous change during source preparation may have introduced this change in composition of that sample.

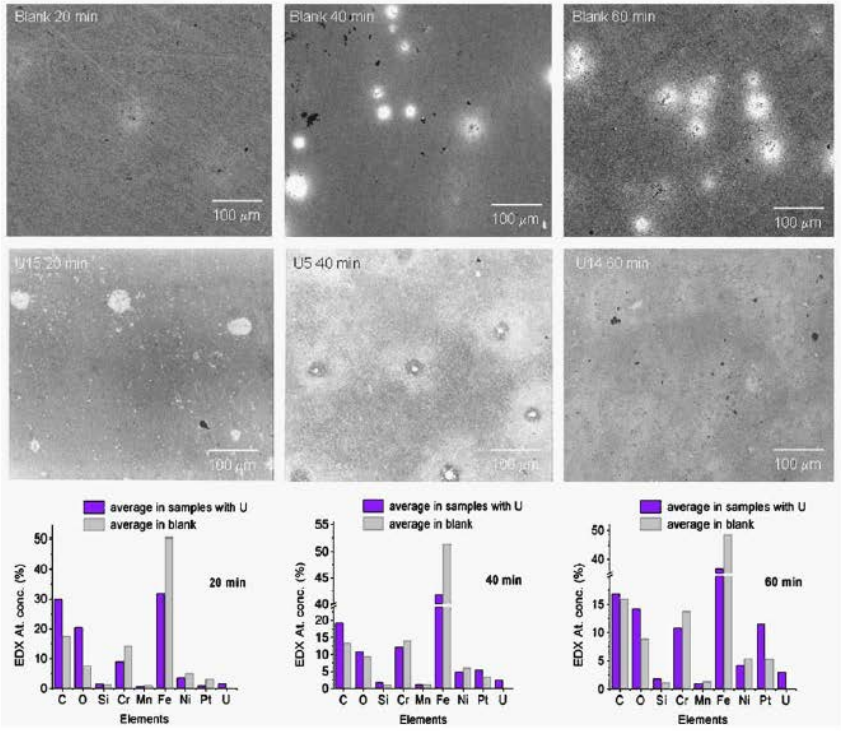

Fig. 2. SEM images for radioactive and blank samples, and semiquantitative results of the EDX analysis on the ten samples presented in Table 1. The numerical results are the average of three or four different equivalent images at SEM-EDX, with amplification 250.

By taking high resolution XPS spectra we further examined the nature of U and Pt species. Fig. 5 (left) contains the high-resolution XP spectra in the spectral regions comprising the U4f (top), the Pt4f (middle) as well as the O1s (bottom) emission lines from all four samples. Note that the 4f emission has always two peaks that arise from spin-orbit coupling of the 4f electrons and results in a lower energy $4f_{7/2}$ and a higher

energy 4f5/2 component. There are small variations in the position of the U4f and O1s peaks across the samples as a function of electrodeposition time, and a clear shift of the Pt4f peaks to higher binding energies (BEs) for samples U13-40 and U4-30. All BE variations as a function of electrodeposition time are summarized in the diagrams on the right of Fig. 5.

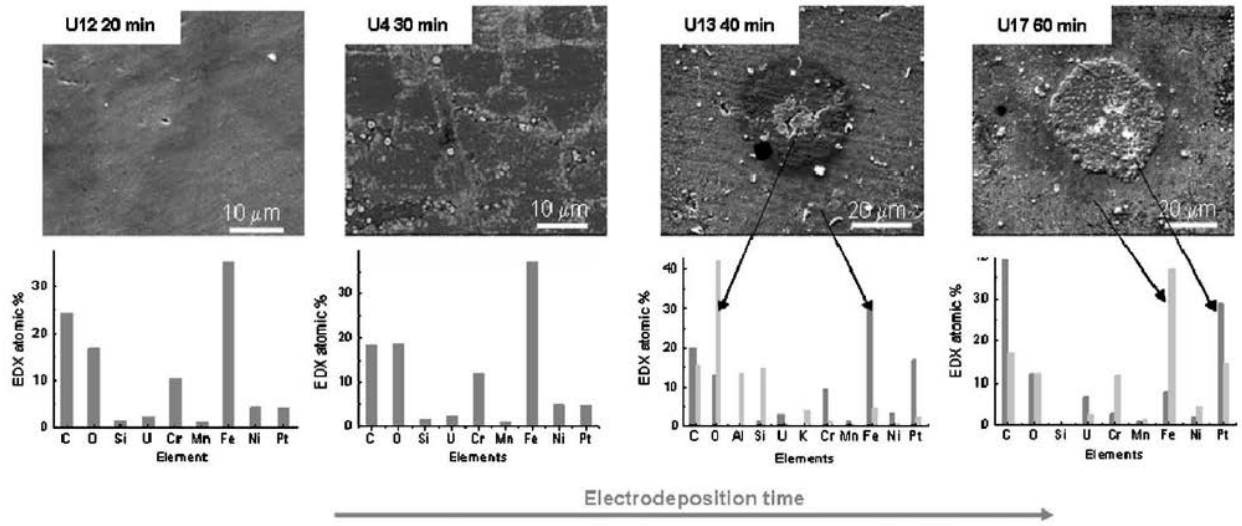

Fig. 3. ESEM images and quantification results of the EDX analysis on uranium sources prepared at different electrodeposition times (from left to right): 20 min (U12-20), 30 min (U4-30), 40 min (U13-40) and 60 min (U17-60).

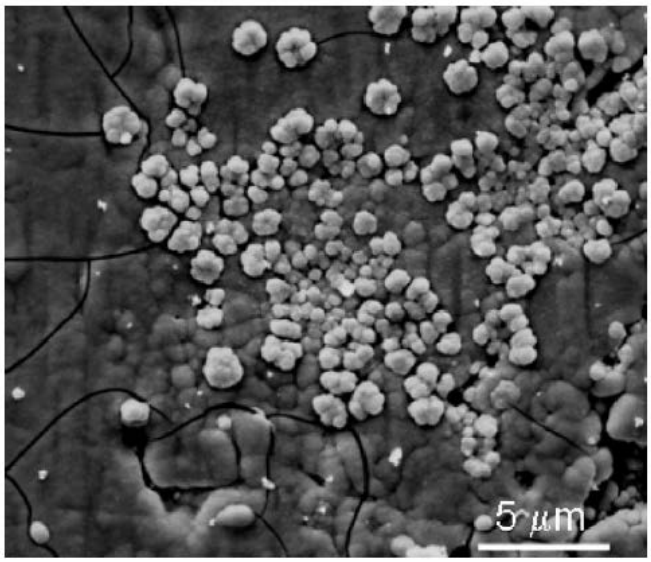

Fig. 4. Magnification of the surface of sample U17-60 illustrating the cracked overlayer and the spherulitic deposits on top.

Table 2
Surface composition obtained from the quantification of the XPS survey spectra.

Peaks	RSF	U12-20 min	U4-30 min	U13-40 min	U17-60 min
O1s	0.630	20.3	20.4	28.0	25.7
U4f	5.600	1.5	0.8	4.3	0.33
C1s	0.205	68.8	59.9	58.3	42.6
Pt4f	1.750	9.3	18.9	9.4	31.4

The RSF factors were taken from (Wagner et al., 1979).

The data analysis was performed fitting single Gauss–Lorentz lines and a Shirley background function (Shirley, 1972) to the U4f, Pt4f and O1s emission lines. The results are summarised in Figs. 6–8. The fitted values for FWHM and BE positions are presented in Table 3. From the literature, there are inherent uncertainties involved with comparing absolute values of BE across different laboratories; therefore it is difficult to assign absolute peak positions to the different oxidation states of uranium. However, the relative distances at which the XPS peak positions should appear for U(IV), U(V) and U(VI) (Chadwick and Graham, 1972; Delobel et al., 1983; Fierro et al., 1985; Allen and Holmes, 1987; Krause et al., 1988; Cox and Farr, 1989; Froideval et al., 2003; Scott et al., 2005) suggest that in our sources uranium is present as a mixture of oxidation states. From the BE positions of the $U4f_{7/2}$ and $U4f_{5/2}$ primary peaks, reduced species (U(IV), U(V)) appear to be predominant in samples U12-20 and U17-60, while in samples U4-30 and U13-40 the contribution from U(VI) species seems higher.

There is strong evidence in the literature indicating that the satellite structure of uranium compounds is in fact a robust indicator of oxidation state and can be used to distinguish U(V) as well as U(IV) and U(VI) (Ilton and Bagus, 2005; Ilton et al., 2005, 2007). The importance of U4f satellite region is that it provides additional information that is not readily apparent in the primary peak envelope. Considering this, we have

also analysed the satellite structure present in our XPS spectra as shown in Fig. 6. The position of these satellite peaks denoted as ‘‘a’’, ‘‘b’’, ‘‘c’’, and ‘‘d’’ with respect to $U4f_{7/2}$ and $U4f_{5/2}$ are presented in Table 4.

From previous work (Bera et al., 1998; Van Den Berghe et al., 2000; Ilton and Bagus, 2005; Ilton et al., 2005, 2007) it is known that both U4f core level peaks show a satellite at ~6.5–7 eV for U(IV), at ~8–8.5 eV for U(V) and two satellites, one at ~4 eV and the other at ~10 eV, for U(VI). In our case, all samples show the U(VI) satellites at ‘‘a’’, ‘‘b’’ and ‘‘d’’ positions and a satellite ‘‘c’’ corresponding to a U(V) state. Due to the broadness of satellite ‘‘c’’ (FWHM ~2 eV), one can argue the presence of mixed species U(IV) and U(V) in particular for samples U12-20 and U17-60 which position ‘‘c’’ lies close to 7 eV. The noise level in sample U17-60 does not allow a clear identification of the satellite ‘‘d’’ feature.

In the case of platinum, the $Pt4f_{7/2}$ peaks at lower BE associated to U12-20 and U17-60 correspond to Pt metal and the Pt XPS peaks associated to U4-30 and U13-40 correspond to PtO (see Table 3)(Kim et al., 1971; Wagner et al., 1979; Fleisch et al., 1985; Legare et al., 1988; He et al., 2007; Kobayashi et al., 2007). It is interesting to note that only sample U17-60 shows a contribution of $Pt4p_{3/2}$ at ~520 eV (see Fig. 8)(Nyholm et al., 1980), suggesting that the amount of Pt in the surface is high. Again, this is also in accordance with the results obtained by alpha spectrometry. The analysis of the O1s shows that all the peak positions are within the range of hydroxyl species (OH^-) BE. This is in agreement with the nature of the deposit in the form of insoluble hydroxides. Indeed, in the seven uranium sources it is observed the shrinkage cracks structure characteristic of U(IV)+U(VI) oxyhydroxides as shown in Fig. 4.

These results demonstrate the sensitivity of the electrodeposi-tion time in the structure of the surface of the alpha sources. In this regard, short (20 min) and long (60 min) electrodeposition times produced a surface containing Pt^0 and U(IV)/U(V) species, while intermediate electrodeposition times of 30 and 40 min produce more oxidised species. Considering that the electrode-position parameters (current intensity, distance between electro-des, sulphuric acid–sodium sulphate electrolyte) were identical during preparation of the sources, with the exception of the electrodeposition time, we may speculate that a progressive oxidation and forced aging of the precipitate occurs in time. This is in agreement with the above-mentioned crusts with shrinkage cracks structure, characteristic of uranium oxyhydroxides, ob-served in all sources. However, surface analysis of sample U17-60 shows the presence of reduced species once again. The explana-tion can be found in Fig. 4 in which the evolution of newly formed spherulitic clusters, containing reduced U and Pt species, towards aged oxidised crusts is observed. Fig. 4 clearly shows the growth of these new spherules on top of a previously deposited oxidised layer.

X-ray absorption fine structure:

Analysis of XAFS spectra were performed using the IFEFFIT (Newville, 2001a) library and its front-ends ATHENA and ARTEMIS (Newville, 2001b; Ravel and Newville, 2005). Theoretical ampli-tudes and phase functions used in the fitting procedure were calculated with FEFF6 (Zabinsky et al., 1995). All the fits were performed using multiple k-weightings of 1, 2 and 3. As result of the XAFS analysis we have obtained information regarding the spatial structure and the uranium oxidation states.

Concerning structure, Fig. 9 shows the uranium L3 XANES spectra of the electrodeposited sources acquired from the centre of the substrates by total-electron-yield. The L_3 absorption edge of uranium arises from the excitation of a $2p_{3/2}$ core electron to the vacant 6d orbitals (major transition in the dipolar approximation)(Hudson et al., 1995). The broad maximum intensity ‘‘whiteline’’ line A (~17171.5 eV for U17-60 and ~17173 eV for U12-20, U4-30 and U13-40) is typical for the uranyl L_3 edge (2p core hole width ¼ 7.4 eV) (Krause and Oliver, 1979). At this edge, the uranyl XANES spectrum is well known to exhibit a characteristic feature B (about ~15–17 eV above the edge maximum) accounting for a strong multiple scattering contribution due to the linear oxo-cation bonds (Petiau et al., 1986; Hudson et al., 1996; Den Auwer et al., 2004). All spectra in Fig. 9 exhibit the uranyl characteristic feature, B. Feature C accounts for the second sphere back-scattering neighbours. The XANES data serve to confirm that in each source the uranyl ion structure is present and hence it provides a reference point for interpreting the EXAFS spectra.

Concerning the uranium oxidation states, based on the literature (Duff et al., 1997; Jernstrom et al., 2004; Salbu et al., 2005; Denecke, 2006; Soldatov et al., 2007), different uranium oxidation states produce UL_3 edge shifts towards higher energies in the order UO_2,U_3O_8,UO_3 due to reduced shielding of the core electrons associated with the increase in mean valence state across the oxidation series. Fig. 9 shows the shift of the absorption edge in the XANES spectra indicating different oxidation states of uranium species in the sources. Based on reported values from the literature (Duff et al., 1997; Jernstrom et al., 2004; Salbu et al., 2005; Denecke, 2006; Soldatov et al., 2007), U17-60 corresponds to U(IV) in agreement with surface studies (XPS), while

U12-20, U4-30 and U13-40 correspond to a mixture of U(V) and U(VI), with U4-30 closer to U(VI).

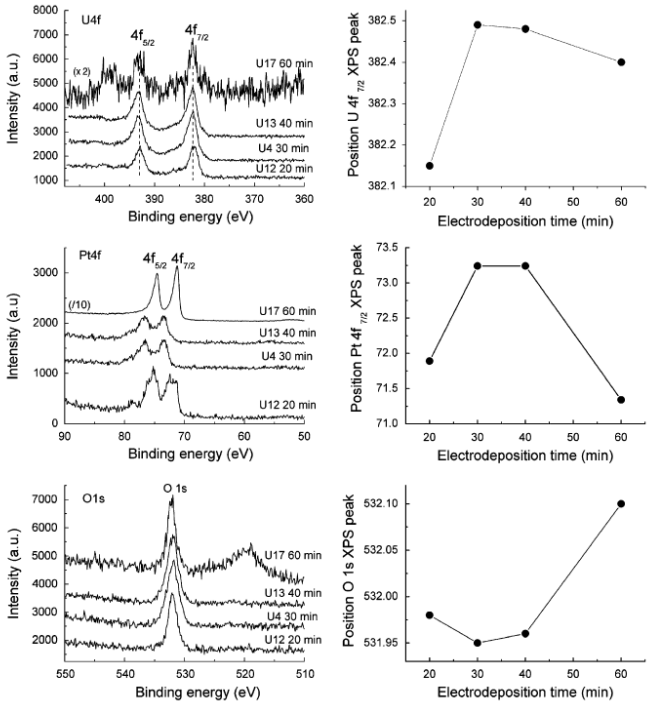

Fig. 5. Left: U4$f_{5/2}$ and 4$f_{7/2}$, Pt4$f_{5/2}$ and 4$f_{7/2}$ and O1s high resolution XPS spectra for the four samples. Right: XPS peak positions plotted as function of the electrodepositing time.

Summarizing the results from XPS and XAFS regarding the uranium oxidation state in the sources it is found that: (i) in all the sources, uranium is present as a mixture of oxidation states; (ii) all the sources show the U(VI) and U(V) contribution, with the contribution of reduced U(IV) species in sources U12-20 and mainly in U17-60; (iii) U4-30 and U13-40 only present oxidised U(V) and U(VI) species.

The EXAFS analysis is shown in Fig. 10 and the fitted values for coordination number N, nearest neighbour distance R and Debye–Waller factor σ^2, are presented in Table 5. The spectra were fitted using the first and second U–O backscattering paths of the α-$UO_2(OH)_2$ centred at 1.792 and 2.496 Å , respectively. A Hanning window determined the k-range and the boundaries of the k^2-weighted Fourier Transform (FT).

All spectra were fitted using multiple k-weightings of 1, 2 and 3. In all cases the Debye–Waller factors were constrained to be lower than 0.002 $Å^2$.

The analysis of the data suggests a uranium atom surrounded by oxygen ligands in the axial and equatorial planes, i.e. an uranyl-type structure. According to Clark et al. (1999) the uranyl structure consists of a uranium ion U(VI) with two O ligands in the axial plane and four or five OH ligands in the equatorial plane, as shown in Fig. 11. EXAFS fitting results indicate that all our samples present these two types of oxygens, axial (Oax) and equatorials (Oeq). In all cases the number of Oeq oxygens is higher than the number of Oax in agreement with the literature (Clark et al., 1999; Vallet et al., 2001; Den Auwer et al., 2003; Catalano et al., 2005). The fitting indicates that these Oax and Qeq correspond to the first and second U–O backscattering paths of the α-$UO_2(OH)_2$ centred at 1.792 and 2.496 Å, respectively. The quality of the data is not good enough to fit a second shell, therefore polymeric species (U–U) (Dos Santos et al., 2004) cannot be ruled out.

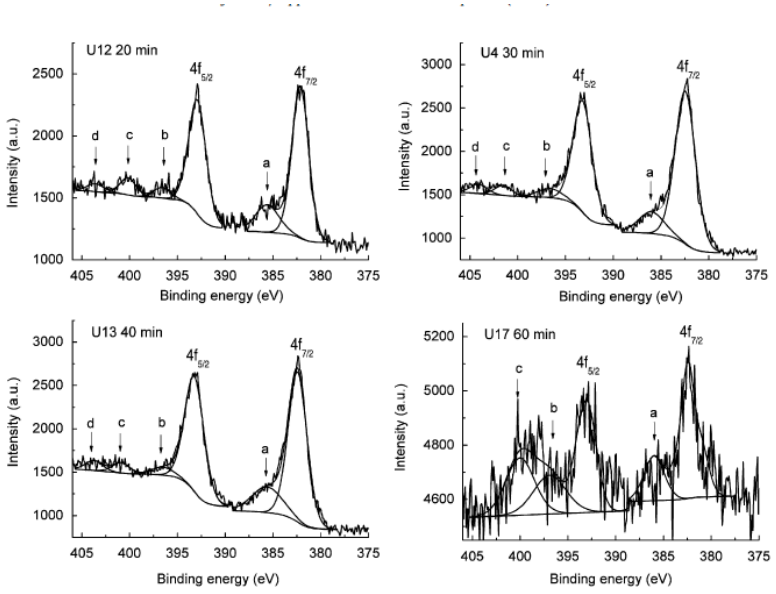

Fig. 6. High-resolution XPS U4$f_{5/2}$ and U4$f_{7/2}$ spectra and single peak fit to the data for the four electrodeposited films. The letters a, b, c and d correspond to the uranium satellite positions according to Table 4.

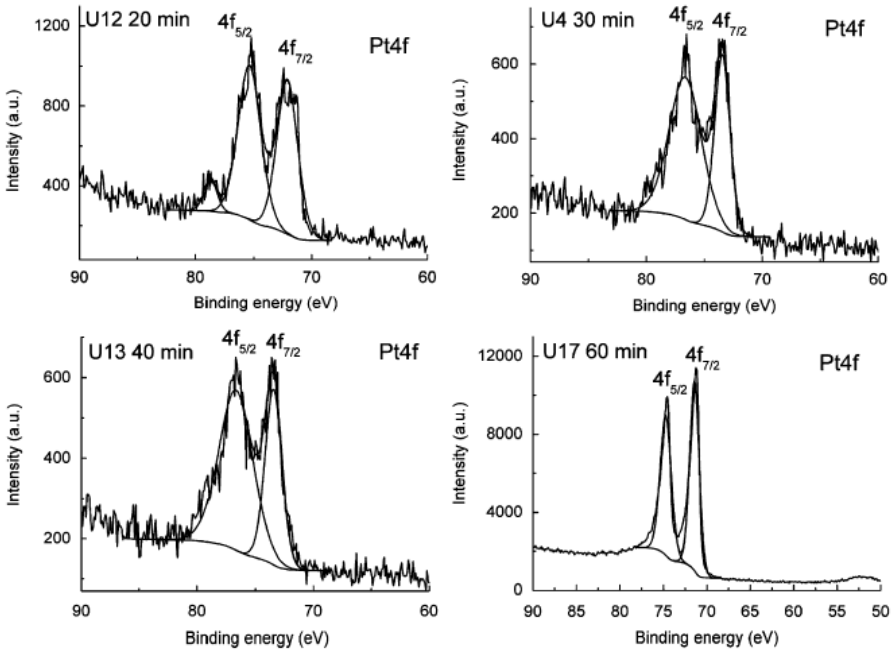

Fig. 7. High-resolution XPS $Pt4f_{5/2}$ and $Pt4f_{7/2}$ spectra and single peak fit to the data for the four electrodeposited films.

From Table 5, sources U12-20 and U4-30 appeared under-coordinated in the equatorial plane and they would be associated with a type ‘‘I’’ (Fig. 11). Samples U13-40 min and U17-60 min seem to correspond to structure ‘‘II’’. This suggests that a large electrodeposition time increases the coordination of uranium species leading to an increase in oxyhydroxides that is reflected by the change of surface morphology as discussed above.

Alpha spectrometry studies:

Fig. 12 shows the alpha spectra obtained from the sources. The main alpha groups of ^{238}U and ^{234}U can be observed. The deterioration of the spectral resolution and peak shifting by an increase in the self-absorption of alpha particles in the deposit is well documented (Garcia-Toran˜o, 2006; Krupa and Kurzak, 1991; Roldán et al., 1994). This effect is clearly observed in the weakest line of the ^{238}U that overlaps the major line

in a degree that depends of the energy resolution. The effect is less evident in the ^{234}U group because of the different alpha energies and probabilities. In fact, peak shifting towards the low-energy part is observed in the spectra from U4-30 and U17-60 but not in the spectrum from U13-40 which also presents good energy resolution. Since the mass of uranium in these four sources is quite similar, the amount of deposited platinum can be responsible for this shifting and the subsequent worsening of the energy resolution. This is in agreement with the XPS surface analysis data that show a low amount of platinum in source U13-40 (see Table 2) and a probable high amount of platinum in the surface of U17-60 (see above).

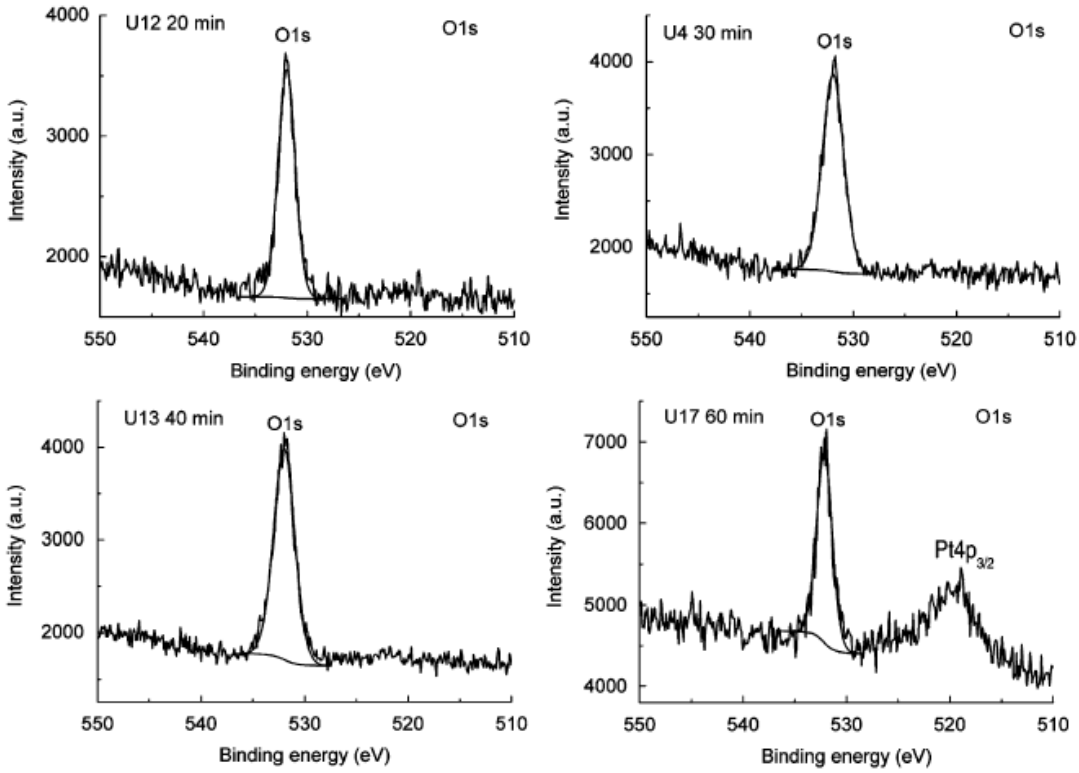

Fig. 8. High-resolution XPS O1s and O1s spectra and single peak fit to the data for the four electrodeposited films.

Table 3
XPS analysis results. Data were fitted using a Gaussian-Lorentzian distribution and the background was modelled using a Shirley (1972) function.

Sample	Peak	FWHM (eV)	Position (eV)
U12 20 min	$U4f_{5/2}$	1.95	392.93
	$U4f_{7/2}$	2.16	382.15
	$Pt4f_{5/2}$	2.30	75.35
	$Pt4f_{7/2}$	2.12	72.10
	O1s	1.90	531.98
U4 30 min	$U4f_{5/2}$	2.48	393.19
	$U4f_{7/2}$	2.68	382.49
	$Pt4f_{5/2}$	3.26	76.63
	$Pt4f_{7/2}$	1.56	73.44
	O1s	2.43	531.95
U13 40 min	$U4f_{5/2}$	2.46	393.29
	$U4f_{7/2}$	2.55	382.48
	$Pt4f_{5/2}$	3.42	76.66
	$Pt4f_{7/2}$	1.71	73.44
	O1s	2.35	531.96
U17 60 min	$U4f_{5/2}$	3.03	393.10
	$U4f_{7/2}$	1.94	382.30
	$Pt4f_{5/2}$	1.49	74.72
	$Pt4f_{7/2}$	1.27	71.41
	O1s	1.78	532.12

Table 4
Position of the U4f satellite peaks shown in Fig. 6.

Sample	Satellite a (eV from $U4f_{7/2}$)	Satellite b (eV from $U4f_{5/2}$)	Satellite c (eV from $U4f_{5/2}$)	Satellite d (eV from $U4f_{5/2}$)
U12-20	3.5	3.6	7.2	10.7
U4-30	3.5	3.6	8.5	11.0
U13-40	3.2	3.6	7.6	10.4
U17-60	3.7	3.9	6.9	Cannot be resolved

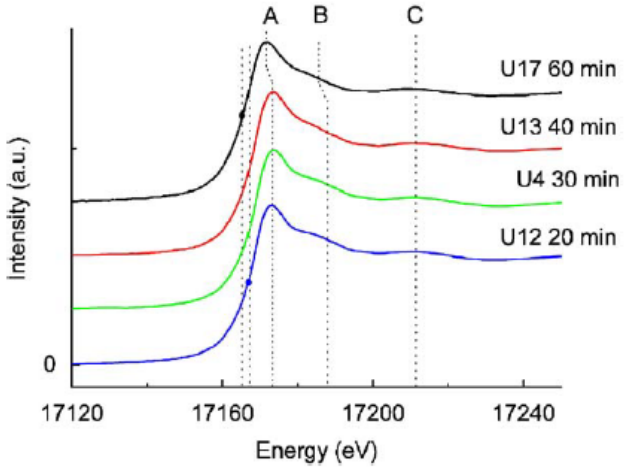

Fig. 9. XANES spectra taken at the UL_3 edge for all electrodeposited films. The figure shows a shift in the spectra of ~1 eV for U17-60 with respect to the other samples. Feature A is the maximum at resonance ("whiteline"), feature B is characteristic of uranyl species and feature C accounts for the second sphere backscattering neighbours.

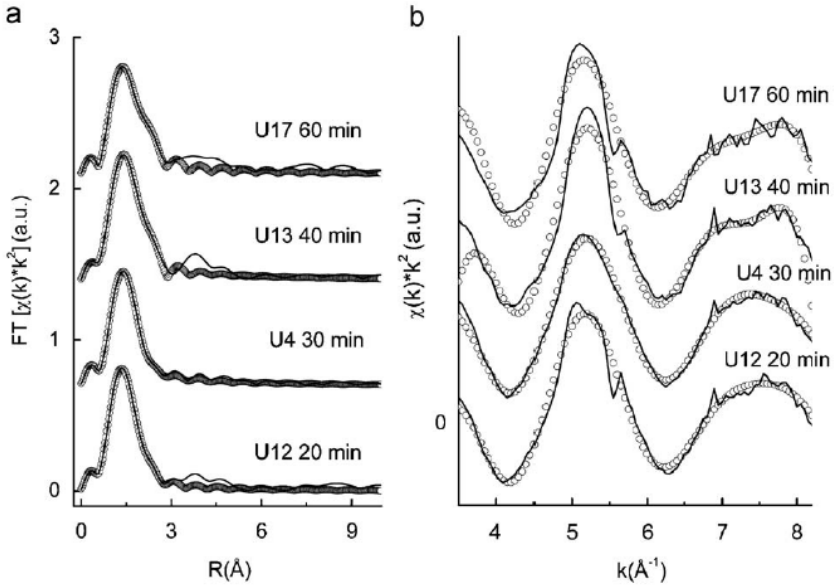

Fig. 10. EXAFS region of the electrodeposited uranium films. The plots show the (a) Fourier Transform $k^2\chi(k)$ function (lines) and the fit (points) and (b) the $k^2\chi(k)$ function (lines) and the correspondent fit (points). The spectra were fitted using the first and second U–O backscattering paths of the α-$UO_2(OH)_2$. A Hanning window determined the k-range and the boundaries of the k^2-weighted Fourier Transform. All spectra were fitted using multiple k-weightings of 1, 2 and 3.

Table 5
Fitted values for coordination number *N*, nearest neighbour distance R and Debye-Waller factor σ^2 obtained from the analysis of the electrodeposited uranium films taken at the UL_3 edge.

Sample	Scattering path	*N*	*R* (Å)	σ^2 (Å^2)	E_0 (eV)	*R* factor	*k*-range (Å^{-1})	FT-range (Å)
U 4 30 min	U–O ax	2.6	1.81	0.006	11.2	0.0002	3.86–8.13	1–2.9
	U–O eq	3.1	2.41	0.008				
U 12 20 min	U–O ax	2.2	1.82	0.003	13.3	0.0001	3.76–8.13	1–2.9
	U–O eq	3.2	2.45	0.008				
U 13 40 min	U–O ax	1.7	1.73	0.003	13.1	0.0016	3.76–8.13	1–2.9
	U–O eq	5.1	2.44	0.004				
U 17 60 min	U–O ax	1.7	1.79	0.003	13.3	0.0013	3.86–8.13	1–2.9
	U–O eq	4.7	2.46	0.007				

The spectra were fitted using the first and second U–O backscattering paths of the α-$UO_2(OH)_2$ centred at 1.792 and 2.496 Å respectively. Errors are ± 10% of the reported value.

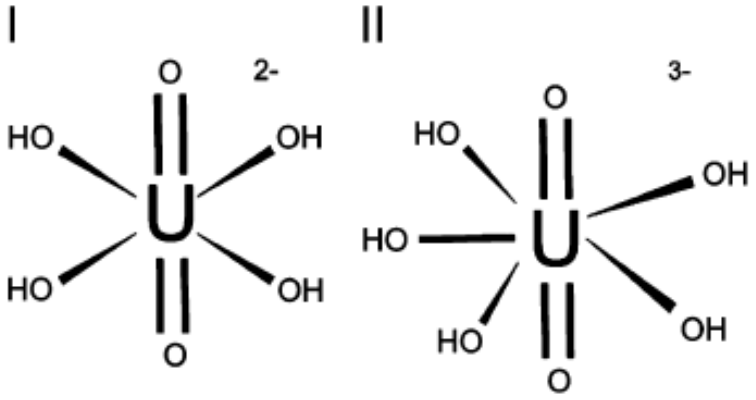

Fig. 11. Uranyl structure showing a uranium ion U(VI) with two O ligands in the axial plane and four or five OH ligands in the equatorial plane, taken from(Clark, 1999).

Conclusions

Alpha sources of uranium prepared by the Hallstadius method, contain Pt atoms which evolve with the electrodeposition time to mossy aggregates, not uniformly distributed on the surface of the substrate. These platinum aggregates contribute to deteriorate the energy resolution of the alpha spectra obtained from the sources, even in the deposition of nuclides such as ^{238}U ($T_{1/2}$ = 4.468 x 10^9 y) (Bé et al., 2006), which contribute with significant mass to the deposit thickness. In the case of short-live

actinides, we may speculate that the behaviour of Pt aggregates would be similar to our blank samples, and energy resolution would be also deteriorated.

SEM and EDX studies carried out on uranium sources indicate that, although U deposition can occur without the interference of Pt when using semipermeable membranes (Ferrero Calabuig et al., 1998b), the porous morphology of the platinum aggregates seems to play an important role in the electrodeposition of the insoluble hydroxides. In line with the Hansen theory, the high specific surface of the Pt deposits appears to favours an increase of the surface hydroxyl concentration, which then provides nucleation sites for subsequent preferential U precipitation.

XPS revealed the sensitivity of the oxidation state of uranium and platinum species on the electrodeposition time. Evidence for the evolution from newly formed reduced to aged oxidised uranium and from Pt to PtO species has been observed. Initially formed spherulitic clusters (on top of the oxidised species), contain reduced U and Pt species, but further growth leads to the formation of oxidised crusts.

XAFS studies confirmed the presence of different uranium oxyhydroxide species in these sources. A large electrodeposition time appears to increase the coordination number of uranium leading to an increase in oxyhydroxide ligands.

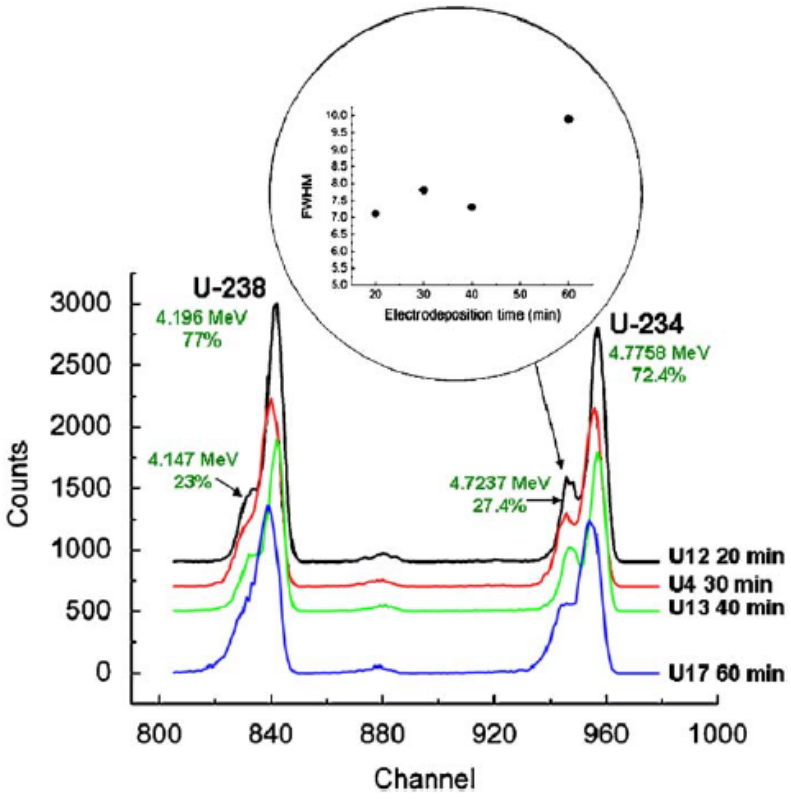

Fig. 12. Alpha spectra of the electrodeposited uranium films. The inset shows the FWHM of a Gaussian fit to the 4.7237 MeV peak as a function of electrodeposition time.

Acknowledgments

This research has been partially supported by SEP-CONACYT project 26040. AMB, NT and SLMS were supported by EPSRC under contract No. GR/S85801/01.We thank STFC (CLRC) for the award of XAFS beamtime (award number 46337).

References

1. - Allen, G.C.,Holmes,N.R.,1987.Surfacecharacterisationof a-, b-, g-, and d-UO3 using X-rayphotoelectronspectroscopy.J.Chem.Soc.,DaltonTrans.1987(12), 3009–3015.

2.- Alonso-Hernandez, C.,Diaz-Asencio,M.,Munos-Caravaca,A.,Suarez-Morell,E., Avila-Moreno,R.,2002.137Csand210Podoseassessmentfrommarinefoodin Cienfuegos Bay(Cuba).J.Environ.Radioact.61(2),203–211.

3.- Álvarez, A., Gascó, C., Navarro, N., Antón, M.P., Sancho, C., 2005. Determination of actinides in samples obtained during dismantling activities. J. Radioanal. Nucl. Chem. 265 (3), 383–387.

4.- Arimoto, R., Webb, J.L., Conley, M., 2005. Radioactive contamination of atmospheric dust over southeastern New Mexico. Atmos. Environ. 39 (26), 4745–4754.

5.- Bé, M.M., Chisté , V., Dulieu, C., Browne, E., Baglin, C., Chechev, V., Kuzmenko, N., Helmer, R., Kondev, F. MacMahon, D., Lee, K.B., 2006. Table of radionuclides, vol. 3—A = 3 to 244, Monographie BIPM-5. Bureau International des Poids et Measures, Pavillon de Breteuil, F-92310 Sévres. ISBN 92-822-2218-7.

4.- Becerril-Vilchis, A., Cortes, A., Dayras, F., de Sanoit, J., 1996. A method for the preparation of very thin and uniform alpha-radioactive sources. NIM A 369 (2), 613–616.

5.- Bera, S., Sali, S.K., Sampath, S., Narasimhan, S.V., Venugopal, V., 1998. Oxidation state of uranium: an XPS study of alkali and alkaline earth uranates. J. Nucl. Mater. 255 (1), 26–33.

6.- Catalano, J.G., Trainor, T.P., Eng, P.J., Waychunas, G.A., Brown Jr., G.E., 2005. CTR diffraction and grazing-incidence EXAFS study of U(VI) adsorption onto α-Al2O3 and a-Fe2 O3 (11?02) surfaces. Geochim. Cosmochim. Acta 69 (14), 3555–3572.

7.- Chadwick, D., Graham, J., 1972. X-ray photoelectron spectra of uranium oxides. Nat. (London) Phys. Sci. 237 (77), 127–128.

8.- Clark, D.L., Conradson, S.D., Donohoe, R.J., Webster Keogh, D., Morris, D.E., Palmer, P.D., Rogers, R.D., Drew Tait, C., 1999. Chemical speciation of the uranyl ion under highly alkaline conditions. Synthesis, structures, and oxo ligand exchange dynamics. Inorg. Chem. 38 (7), 1456–1466.

9.- Clark, D.L., Conradson, S.D., Donohoe, S.J., Keogh, D.W., Morris, D.E., Palmer, P.D., Rogers, R.D., Tait, C.D., 1999. Inorg. Chem. 38, 1456–1466.

10.- Cox, L.E., Farr, J.D., 1989. 4f binding-energy shifts of the light-actinide dioxides and tetrafluorides. Phys. Rev. B 39 (15), 11142–11145.

11.- Crespo, M.T., Perez Del Villar, L., Quejido, A.J., Sanchez, M., Cozar, J.S., Fernandez- Diaz, M., 2003. U-series in Fe–U-rich fracture fillings from the oxidised cap of the ‘‘Mina Fe’’ uranium deposit (Spain): implications for processes in a radwaste repository. Appl. Geochem. 18 (8), 1251–1266.

12.- Danesi, P.R., Bleise, A., Burkart, W., Cabianca, T., Campbell, M.J., Makarewicz, M., Moreno, J., Tuniz, C., Hotchkis, M., 2003. Isotopic composition and origin of uranium and plutonium in selected soil samples collected in Kosovo. J. Environ. Radioact. 64 (2–3), 121–131.

13.- Delobel, R., Baussart, H., Leroy, J.M., Grimblot, J., Gengembre, L., 1983. X-ray photoelectron spectroscopy study of uranium and antimony mixed metal-oxide catalysts. J. Chem. Soc., Faraday Trans. 79 (4), 879–891.

14.- Den Auwer, C., Guillaumont, D., Guilbaud, P., Conradson, S.D., Rehr, J.J., Ankudinov, A., Simoni, E., 2004. Theoretical chemical contribution to the simulation of the LIII X-ray absorption edges of uranyl, neptunyl and osmyl hydrates and hydroxides. New J. Chem. 28 (8), 929–939.

15.- Den Auwer, C., Simoni, E., Conradson, S., Madic, C., 2003. Investigating actinyl oxo cations by X-ray absorption spectroscopy. Eur. J. Inorg. Chem. (21), 3843–3859.

16.- Denecke, M.A., 2006. Actinide speciation using X-ray absorption fine structure spectroscopy. Coord. Chem. Rev. 250 (7–8), 730–754.

17.- Dos Santos, L.R., Sbampato, M.E., Dos Santos, A.M., 2004. Characterization of electrodeposited uranium films. J. Radioanal. Nucl. Chem. 261, 203–209.

18.- Duff, M.C., Amrhein, C., Bertsch, P.M., Hunter, D.B., 1997. The chemistry of uranium in evaporation pond sediment in the San Joaquin Valley, California, USA, using X-ray fluorescence and XANES techniques. Geochim. Cosmochim. Acta 61 (1), 73–81.

19.- Fairley, N., 1999–2002. CasaXPS Casa Software Ltd.

20.- Ferrero Calabuig, J.L., Martin Sanchez, A., Roldan Garcia, C., Rosello Ferrando, J., Da Silva, M.F., Soares, J.C., Vera Tome, F., 1996. Characterization of alpha sources by Rutherford backscattering spectrometry. NIM A 369 (2–3), 603–607.

21.- Ferrero Calabuig, J.L., Vera Tome, F., Martin Sanchez, A., Roldan Garcia, C., Da Silva, M.F., Soares, J.C., Ager, F.J., Juanes Barber, D., Rubio Montero, P., 1998a. Ion beam analysis and alpha spectrometry of sources electrodeposited on several backings. NIM B 136–138, 290–296.

22.- M.F., Soares, J.C., Ager, F.J., Juanes Barber, D., Rubio Montero, P., 1998a. Ion beam analysis and alpha spectrometry of sources electrodeposited on several backings. NIM B 136–138, 290–296.

23.- Ferrero Calabuig, J.L., Martin Sanchez, A., Roldan Garcia, C., Vera Tome, F., Da Silva, M.F., Soares, J.C., Juanes Barber, D., 1998b. Semipermeable membrane to retain platinum atoms in the electrodeposition process of alpha spectrometry sources. Appl. Radiat. Isot. 49 (9–11), 1269–1272.

24.- Fierro, J.L.G., Salazar, E., Legarreta, J.A., 1985. Characterization of silica-supported uranium–molybdenum oxide catalysts. Surf. Interface Anal. 7 (2), 97–104.

25.- Fleisch, T.H., Zajac, G.W., Schreiner, J.O., 1985. XPS study of the uv photoreduction of transition and noble metal oxides. Appl. Surf. Sci. 26 (4), 488–497.

26.- Froideval, A., Del Nero, M., Barillon, R., Hommet, J., Mignot, G., 2003. pH dependence of uranyl retention in a quartz/solution system: an XPS study. J. Colloid Interface Sci. 266 (2), 221–235.

27.- Garcia-Torano, E., 2006. Current status of alpha-particle spectrometry. Appl. Radiat. Isot. 64 (10–11), 1273–1280.

28.- Garcia-Torano, E., Crespo, M.T., Roteta, M., Sibbens, G., Pomme, S., Sanchez, A.M., Montero, M.P.R., Woods, S., Pearce, A., 2005. α-particle emission probabilities in the decay of 235U. NIM A 550 (3), 581–592.

29.- Gascon, J.L., Acena, M.L., Suarez, J.A., Rodriguez, M., 1994. Radiochemical methods for the determination of plutonium, americium and curium in typical waste streams. J. Alloys Compd. 213–214, 557–559.

30.- Hallstadius, L., 1984. A method for the electrodeposition of actinides. NIM Phys. Res. 223 (2–3), 266–267.

31.- Hansen, P.G., 1959. The conditions for electrodeposition of insoluble hydroxides at a cathode surface: a theoretical investigation. J. Inorg. Nucl. Chem. 12, 30–37.

32.- He, B., Ha, Y., Liu, H., Wang, K., Liew, K.Y., 2007. Size control synthesis of polymer- stabilized water-soluble platinum oxide nanoparticles. J. Colloid Interface Sci. 308 (1), 105–111.

33.- Hudson, E.A., Allen, P.G., Terminello, L.J., Denecke, M.A., Reich, T., 1996. Polarized X- ray-absorption spectroscopy of the uranyl ion: comparison of experiment and theory. Phys. Rev. B 54 (1), 156–165.

34.- Hudson, E.A., Rehr, J.J., Bucher, J.J., 1995. Multiple-scattering calculations of the uranium L3-edge X-ray-absorption near-edge structure. Phys. Rev. B 52 (19), 13815–13826.

35.- Ilton, E.S., Bagus, P.S., 2005. Many-body effects in the 4f X-ray photoelectron spectroscopy of the U5+ and U4+ free ions. Phys. Rev. B 71, 195121.

36.- Ilton, E.S., Haiduc, A., Cahill, C.L., Felmy, A.R., 2005. Mica surfaces stabilize pentavalent uranium. Inorg. Chem. 44 (9), 2986–2988.

37.- Ilton, E.S., Boily, J.F., Bagus, P.S., 2007. Beam induced reduction of U(VI) during X-ray photoelectron spectroscopy: the utility of the U4f satellite structure for identifying uranium oxidation states in mixed valence uranium oxides. Surf. Sci. 601 (4), 908–916.

38.- Jernstrom, J., Eriksson, M., Osan, J., Tamborini, G., Torok, S., Simon, R., Falkenberg, G., Alsecz, A., Betti, M., 2004. Non-destructive characterisation of low radioactive particles from Irish Sea sediment by micro X-ray synchrotron radiation techniques: micro X-ray fluorescence (m-XRF) and micro X-ray absorption near edge structure (m-XANES) spectroscopy. J. Anal. At. Spectrom. 19 (11), 1428–1433.

39.- Kim, K.S., Winograd, N., Davis, R.E., 1971. Electron spectroscopy of platinum–oxygen surfaces and application to electrochemical studies [22]. J. Am. Chem. Soc. 93 (23), 6296–6297.

40.- Kobayashi, M., Morita, A., Ikeda, M., 2007. The support effect in oxidizing atmosphere on propane combustion over platinum supported on TiO2, TiO2–SiO2 and TiO2–SiO2–WO3. Appl. Catal. B: Envion. 71 (1–2), 94–100.

41.- Koningsberger, D.C., Prins, R.E., 1988. X-ray Absorption: Principles, Applications, Techniques of EXAFS, SEXAFS, and XANES. Wiley, New York, NY, USA.

42.- Krause, M.O., Haire, R.G., Keskirahkonen, O., Peterson, J.R., 1988. Photoelectron spectrometry of the actinides from Ac to Es. J. Electron. Spectrosc. Relat. Phenom. 47, 215–226.

43.- Krause, M.O., Oliver, J.H., 1979. Natural widths of atomic K and L levels, K alpha X-ray lines and several KLL Auger lines. J. Phys. Chem. Ref. Data 8 (2), 329–338.

44.- Krupa, R.J., Kurzak, K., 1991. Simulation and evaluation of [alpha]-spectra obtained with semiconductor detectors. NIM A 307 (2–3), 469–483.

45.- Lee, M.H., Lee, C.W., 2000. Preparation of alpha-emitting nuclides by electro-deposition. NIM A 447 (3), 593–600.

46.- Legare, P., Lindauer, G., Hilaire, L., Maire, G., Ehrhardt, J.J., Jupille, J., Cassuto, A., Guillot, C., Lecante, J., 1988. On the interaction of O-2 with Pt(111) and Pt(5 5 7) surfaces-core-level shift study using conventional and synchrotron radiation sources. Surf. Sci. 198 (1–2), 69–78.

47.- Martin Sanchez, A., Nuevo, M.J., Jurado Vargas, M., Diaz Bejarano, J., da Silva, M.F., Roldan Garcia, C., Paul, A., Ferrero Calabuig, J.L., Mendez Vilas, A., Juanes Barber, D., 2002a. Application of atomic and nuclear techniques to the study of inhomogeneities in electrodeposited alpha-particle sources. NIM B 190, 747–750.

48.- Martin Sanchez, A., Nuevo Sanchez, M.J., Rubio Montero, M.P., Mendez Vilas, A., 2002b. Study of inhomogeneities in sources prepared for alpha-particle spectrometry using scanning probe microscopy. Appl. Radiat. Isot. 56 (1–2), 31–36.

49.- Minteer, M., Winkler, P., Wyatt, B., Moreland, S., Johnson, J., Winters, T., 2007. Reliability of using U-238/U-235 and U-234/U-238 ratios from alpha spectro-metry as qualitative indicators of enriched uranium contamination. Health Phys. 92 (5), 488–495.

50.- Newville, M., 2001a. IFEFFIT: interactive XAFS analysis and FEFF fitting. J. Synch. Rad. 8 (2), 322–324.

51.- Newville, M., 2001b. EXAFS analysis using FEFF and FEFFIT. J. Synch. Rad. 8 (2), 96–100.

52.- Nyholm, R., Berndtsson, A., Martensson, N., 1980. Core level binding energies for the elements Hf to Bi (Z ¼ 72–83). J. Phys. C Solid State Phys. 13 (36).

53.- O'Connor, D.J., Sexton, B.A., Smart, R.S.C., 2003. Surface Analysis Methods in Materials Science. Springer, Berlin.

54.- Ota, K.I., Nishigori, S., Kamiya, N., 1988. Dissolution of platinum anodes in sulfuric acid solution. J. Electroanal. Chem. Interfacial Electrochem. 257 (1), 205–215.

55.- Pavlovic, M.G., Popov, K.I., 2005. Metal powder production by electrolysis. In: Nagy, Z. (Ed.), Electrochemistry Encyclopedia /http://electrochem.cwru.edu/ed/encycl/art-p04-metalpowder.htmS. Yeager Center for Electrochemical Sciences Chemical Engineering Department, Case Western Reserve University Cleveland, Ohio.

56.- Perez del Villar, L.P., Bruno, J., Campos, R., Gomez, P., Cozar, J.S., Garralon, A., Buil, B., Arcos, D., Carretero, G., Ruiz Sanchez-Porro, J., Hernan, P., 2002. The uranium ore from Mina Fe (Salamanca, Spain) as a natural analogue of processes in a spent fuel repository. Chem. Geol. 190 (1–4), 395–415.

57.- Petiau, J., Calas, G., Petitmaire, D., Bianconi, A., Benfatto, M., Marcelli, A., 1986. Delocalized versus localized unoccupied 5f states and the uranium site structure in uranium oxides and glasses probed by X-ray-absorption near-edge structure. Phys. Rev. B 34 (10), 7350–7361.

58.- Ramdohr, P., 1969. The Ore Minerals and their Intergrowths. Pergamon Press Oxford, UK.

59.- Ravel, B., Newville, M., 2005. ATHENA, ARTEMIS, HEPHAESTUS: data analysis for X-ray absorption spectroscopy using IFEFFIT. J. Synch. Rad. 12 (4), 537–541.

60.- Renteria Villalobos, M., Montero Cabrera, M.E., Reyes Cortes, M., Herrera Peraza, E.F., Rodriguez Pineda, A., Monjon Collado, G., Garcia Tenorio, R., Crespo, T., Valenzuela Hernandez, M., 2007. Characterization of source rocks and groundwater radioactivity at the Chihuahua valley. Revista Mexicana de Fı´sica 53 (3), 16–22.

61.- Roldan, C., Ferrero, J.L., Sanchez, F., Navarro, E., Rodriguez, M.J., 1994. Monte Carlo simulation of alpha spectra in low-geometry measurements. NIM A 338 (2–3), 506–510.

62.- Rubio Montero, M.P., Martı´nS´anchez, A., Carrasco Lourtau, A.M., 2004. Isotopic uranium and plutonium analysis by alpha-particle spectrometry. NIM B 213 (1), 429–433.

63.- Salbu, B., Janssens, K., Lind, O.C., Proost, K., Gijsels, L., Danesi, P.R., 2005. Oxidation states of uranium in depleted uranium particles from Kuwait. J. Environ. Radioact. 78 (2), 125–135.

64.- Scott, T.B., Allen, G.C., Heard, P.J., Randell, M.G., 2005. Reduction of U(VI) to U(IV) on the surface of magnetite. Geochim. Cosmochim. Acta 69 (24), 5639–5646.

65.- Serrano, K., Taxil, P., Dugne, O., Bouvet, S., Puech, E., 2000. Preparation of uranium by electrolysis in chloride melt. J. Nucl. Mater. 282 (2–3), 137–145.

66.- Shirley, D.A., 1972. High-resolution X-ray photoemission spectrum of the valence bands of gold. Phys. Rev. B 5 (12), 4709–4714.

67.- Sill, C.W., 1987. Determination of radium-226 in ores, nuclear wastes and environmental samples by high-resolution alpha spectrometry. Nucl. Chem. Waste Manage. 7 (3–4), 239–256.

68.- Soldatov, A.V., Lamoen, D., Konstantinovic, M.J., Van den Berghe, S., Scheinost, A.C., Verwerft, M., 2007. Local structure and oxidation state of uranium in some ternary oxides: X-ray absorption analysis. JSSC 180 (1), 54–61.

69.- Talvitie, N.A., 1972. Electrodeposition of actinides for alpha spectrometric determination. Anal. Chem. 44 (2), 280–283.

70.- Tsoupko-Sitnikov, V., Dayras, F., De Sanoit, J., Filossofov, D., 2000. Application of rotating disk electrode technique for the preparation of Np, Pu and Am a- sources. Appl. Radiat. Isot. 52 (3), 357–364.

71.- Vallet, V., Wahlgren, U., Schimmelpfennig, B., Moll, H., Szabo, Z., Grenthe, I., 2001.

72.- Solvent effects on uranium(VI) fluoride and hydroxide complexes studied by EXAFS and quantum chemistry. Inorg. Chem. 40 (14), 3516–3525. +

73.- Van Den Berghe, S., Laval, J.P., Gaudreau, B., Terryn, H., Verwerft, M., 2000. XPS investigations on cesium uranates: mixed valency behaviour of uranium. J. Nucl. Mater. 277 (1), 28–36.

74.- Vera Tomé , F., Martin Sa´ nchez, A., 1991. Optimizing the parameters affecting the yield and energy resolution in the electrodeposition of uranium. Appl. Radiat. Isot. 42, 135–140.

75.- Vera Tome´ , F., Jurado Vargas, M., Martin Sa´ nchez, A., 1994. SIMPLEX method for

optimization of experiments: application to electrodeposition in alpha spectrometry. NIMPA 348, 183–187.

76.- Wagner, C.D., Riggs, W., Davis, L., Moulder, J., 1979. Handbook of X-ray photoelectron spectroscopy: a reference book of standard data for use in X-ray photoelectron spectrocopy. Perkin-Elmer, Eden Prairie, Minnesota.

77.- Wang, R.Y., Kirk, D.W., Zhang, G.X., 2006. Effects of deposition conditions on the morphology of zinc deposits from alkaline zincate solutions. J. Electrochem. Soc. 153 (5).

78.- Weber, R., Vater, P., Esterlund, R.A., Patzelt, P., 1999. On the energy resolution of alpha-sources prepared by electrodeposition of uranium. NIM A 423 (2–3), 468–471.

79.- Yamamoto, M., Kawabata, Y., Murata, Y., Komura, K., 2002. Variation of uranium isotopic composition in soil within the JCO grounds from the 30 September 1999 criticality accident at JCO, Tokai-Mura, Japan. Health Phys. 83 (2), 197–203.

80.- Zabinsky, S.I., Rehr, J.J., Ankudinov, A., Albers, R.C., Eller, M.J., 1995. Multiple-scattering calculations of X-ray-absorption spectra. Phys. Rev. B 52 (4), 2995–3009.